Tribocorrosion Framework of (Iron, Nickel, Zinc)-Doped Graphene Nanosheet: New Sights into Sulfur Dioxide and Hydrogen Sulfide Removal Using DFT/TD-DFT Methods

Fatemeh Mollaamin[1,2] · Majid Monajjemi[3]

Abstract

Progress of largely selective and sensitive compounds is essential for removing two toxic gases of hydrogen sulfide (H_2S) and sulfur dioxide (SO_2).The effect of Iron (Fe), Nickel (Ni), and Zinc (Zn) doping of graphene (Gr) nanosheet (NS) on their adsorption for both H_2S and SO_2 gases has been investigated in this work using first-principles density-functional theory (DFT) computations. In this research, it has been investigated the ability of transition metals of iron, nickel, and zinc doping of Gr@NS for adsorption toxic gas of Sulfur Dioxide and Hydrogen Sulfide Removal. The Langmuir adsorption model with a three-layered ONIOM used CAM-B3LYP functional accompanying LANL2DZ and 6–31＋G (d,p) basis sets due to Gaussian 16 revision C.01 program on the complexes of H_2S and $SO_2 \rightarrow TM$(Fe, Ni, Zn) doping of Gr nanosheet. The changes of charge density have shown the values of $\Delta Q_{\text{Fe-doped}} = -0.566 >> \Delta Q_{\text{Zn-doped}} = +0.387 >>> \Delta Q_{\text{Ni-doped}} = +0.605$ for H_2S adsorption and $\Delta Q_{\text{Fe-doped}} = -0.336 >> \Delta Q_{\text{Zn-doped}} = +0.376 >>> \Delta Q_{\text{Ni-doped}} = +0.618$ for SO_2 adsorption. Based on these amount of changes of charge density, H_2S and SO_2 have exhibited a significant charge transfer for Fe doping of graphene nanosheet compared to Ni- and Zn-doped Gr@NS. Based on NMR spectroscopy, it has been illustrated that the sharp peaks in the adsorption site are due to the Fe, Ni, and Zn doping on the surface of graphene nanosheet through H_2S and SO_2 adsorption. However, it has represented some fluctuations in the chemical shielding of isotropic and anisotropy behaviors around Zn-doped on the $H_2S/ SO_2 \rightarrow$ Zn-doped/Gr@NS. Moreover, it has exhibited the fluctuation of occupancy of NBO for $H_2S/ SO_2 \rightarrow$ Fe-doped, $H_2S/SO_2 \rightarrow$ Ni-doped, and $H_2S/SO_2 \rightarrow$ Zn-doped graphene nanosheet through the Langmuir adsorption process by indicating the active sulfur atom in hydrogen sulfide (H_2S) and sulfur dioxide (SO_2) becoming close to the nanosheet. The amounts of $\Delta G^{\text{o}}_{\text{ads}}$ through IR computations based on polarizability have exhibited that $\Delta G^{\text{o}}_{\text{ads,SO2} \rightarrow \text{Fe–C}}$ and $\Delta G^{\text{o}}_{\text{ads,H2S} \rightarrow \text{Fe–C}}$ have exhibited the most energy gap because of charge density transfer from sulfur atom in hydrogen sulfide (H_2S) and sulfur dioxide (SO_2) to Fe doping of Gr@NS, although, $\Delta G^{0}_{\text{H2S/SO2} \rightarrow \text{Zn–C}} > \Delta G^{0}_{\text{H2S/SO2} \rightarrow \text{Ni–C}} > \Delta G^{0}_{\text{H2S/SO2} \rightarrow \text{Fe–C}}$. Frontier molecular orbitals of HOMO, LUMO, and band energy gap accompanying some chemical reactivity parameters have represented the attributes of molecular electrical transport of TM (Fe, Ni, Zn) doping of Gr nanosheet for adsorption of H_2S and SO_2 gases. Our results have provided a favorable understanding of the interaction between TM doping of Gr@NS nanosheet and H_2S and SO_2 molecules. A high performance of TM doping of Gr@NS as gas sensor is demonstrated by modeling the material's transport characteristics by means of the Langmuir adsorption and three-layered ONIOM/DFT method. Furthermore, the results of partial electron density of states (PDOS) have confirmed an obvious charge accumulation between the graphene nanosheet and doped atoms of Fe, Ni, and Zn through adsorption of H_2S and SO_2 molecules on the surface due to the recognition of the conduction band region. Finally, this research can build up our knowledge about the electronic structure, relative stability, and surface bonding of various metal-doped graphene nanosheets, metal alloy surfaces, and other dependent mechanisms, like heterogeneous catalysis, friction lubrication, and biological systems.

Keywords Gas sensor · (Fe, Ni, Zn) doping of Gr@NS · H_2S · SO_2 · Toxic gases · ONIOM/DFT · Langmuir adsorption

1 Introduction

There are different practical applications of carbon nano-structures, such as hydrogen adsorption, pollutant molecules adsorption, and gas sensor devices [1–9].

Sensing and grabbing toxic and harmful gases like CO, CO_2, NO, N_2O, CH_4, SO_2, and H_2S can largely help maintain the human health and the ecosystem [10–12]. These days many materials like carbon-based materials have been investigated and applied for adsorptive removal of toxic gases [13–17]. Therefore, it is essential to make high-implement gas sensors for detecting the toxic gases.

Therefore, remarkable surface of carbon nanostructures is a privileged factor for gas sensing and gas adsorption devices. In addition, the enough doping of these compounds with transition metals might enhance their adsorption ability and adjust their selective adsorption as the excellent dopant applicants [18–22].

Moreover, the recent researches have shown that vacancy defects on the metal surface have an important effect on the incidence of hydrogen breaking. So, the adsorption and dissociation mechanism of H_2S and the diffusion action of hydrogen atoms can gently enhance the reactivity of the vacancy defective metal surface [23–25]. Besides, the study on the surface has depicted that the different dissociation behaviors of H_2S on the different surfaces depend not only on the electronic properties of the surfaces, but also on the adsorption configurations of the transition states [26, 27].

Thus, this research wants to investigate the adsorption of hazardous gases such as H_2S and SO_2 using carbon nanostructures decorated by transition metals of iron, nickel, and zinc based on the density-functional theory (DFT) to discover the adsorption parameters of the various TM doping of Gr@NS.

2 Materials, Theoretical Background, and Computational Method

2.1 Adsorptive Removal of Toxic Gases

This article discusses Sulfur Dioxide and Hydrogen Sulfide adsorption on the transition metals. The chapter illustrates the principal mechanisms of bonding occurring during H_2S and SO_2 chemisorption and reviews the results obtained for H_2S and SO_2 adsorption on tungsten. The data on tungsten surfaces are compared with the few results available for H_2S and SO_2 adsorption on molybdenum and chromium. Bonding of the H_2S and SO_2 molecules to a transition metal atom, either in a carbonyl complex or possibly on a metal surface, can be visualized first proceeding by the donation of the lone pair on the carbon atom into vacant d orbitals of the metal atom. The donor ability of H_2S and SO_2 in this manner is known to be extremely small and stabilization of the metal–carbon bond is believed to be obtained by back-donation of electrons from filled d orbitals on the metal into vacant antibonding π^* orbitals on the H_2S and SO_2 molecule. It is thought that the two mechanisms, donation and back-donation, tend to enhance each other in a synergic manner.
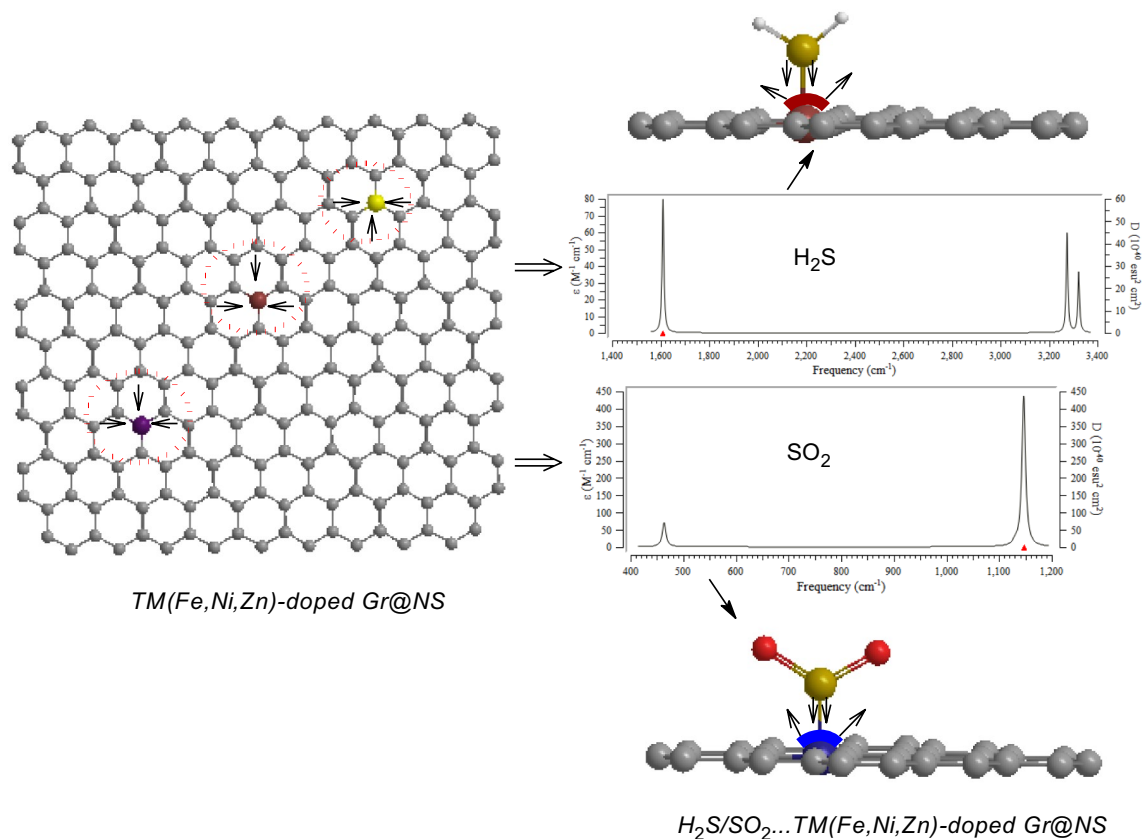
2.2 Langmuir Adsorption Model and Charge Density Analysis

It can be defined the Langmuir adsorption through a physico-chemical interaction on the area of the homogeneous solid state that adsorb compounds without any interactions with each other making a monolayer of molecules on the surface of the solid state. The Langmuir adsorption equation is as the following [28]:

$$\theta_A = \frac{V}{V_m} = \frac{K_{eq}^A p_A}{1 + K_{eq}^A p_A},$$

where θ_A is the fractional occupancy of the adsorption sites; the ratio of V, the volume of gas adsorbed onto the solid, to V_m, the volume of a gas molecules monolayer coating the entire surface of the solid and totally filled by the adsorbate. A continuous monolayer of adsorbate molecules coating a homogeneous solid surface is the conceptual basis for this adsorption system [29, 30]. Different studies have concentrated on the gas adsorption susceptibilities of carbon nanosurfaces which denote a good agreement with the Langmuir adsorption model. The adsorption of toxic H_2S and SO_2 gases on the Fe, Ni, and Zn doping of Gr@NS has been assigned by the most suitable Langmuir isotherm, which exhibits the chemisorptive nature of the bond between $H - \ddot{S} : -H$ and $: \ddot{O} = \ddot{S} = O\ddot{} :$ molecules and TM doping of Gr@NS, the equilibrium electron distribution of the adsorbing compound between the solid and gas phases, and a monolayer attribute. The adsorbed H_2S and SO_2 molecules are kept on TM doping of Gr@NS with Langmuir chemisorption (Scheme 1).

In fact, the nature of the gas sensing mechanism in TM (Fe, Ni, Zn) doping of Gr@NS would be due to charge transfer between surface and H_2S-and SO_2-adsorbed molecules. The changes of charge density analysis in the adsorption process have illustrated that Fe, Ni, and Zn doping of Gr@NS shows the Mulliken charge of − 1.345, − 2.087, and − 1.416, respectively, before adsorption of hydrogen sulfide (H_2S) and − 1.911, − 1.482, and − 1.029, respectively, after adsorption of H_2S. In addition, Fe, Ni, and Zn doping of Gr@NS shows the Mulliken charge of − 1.681, − 1.469,

Scheme 1 Langmuir adsorption of H_2S and SO_2 as the toxic gas pollutant onto TM (Fe, Ni, Zn) doping of Gr@NS

and -1.040, respectively, after adsorption of sulfur dioxide (SO_2).

Therefore, the changes of charge density for Langmuir adsorption of H_2S on Fe, Ni, and Zn doping of Gr@NS alternatively are $\Delta E_{Ni\text{-}doped} = +0.605 >> \Delta E_{Zn\text{-}doped} = +0.387 >>> \Delta E_{Fe\text{-}doped} = -0.566$. The values of changes of charge density have shown a more significant charge transfer for Fe doping of Gr@NS, while H_2S is adsorbed by the metal-doped graphene surface. Furthermore, the changes of charge density for Langmuir adsorption of SO_2 on Fe, Ni, and Zn doping of Gr@NS alternatively are $\Delta E_{Ni\text{-}doped} = +0.618 >> \Delta E_{Zn\text{-}doped} = +0.376 >>> \Delta E_{Fe\text{-}doped} = -0.336$. In fact, the values of changes of charge density have also indicated a more distinct charge transfer for Fe doping of Gr@NS through SO_2 adsorption.

2.3 ONIOM/DFT Method

The combination of three levels in decreasing order of accuracy has been defined, including high, medium, and low levels of theory. High level has been done using the DFT method of Cam-B3LYP with 6–31 + G (d,p) basis set for oxygen, sulfur, and LANL2DZ for transition metals

of iron, nickel, and zinc in the adsorption sites. Medium level has been done on some carbon atoms of graphene in the adsorption site due to semi-empirical methods. Finally, a low level has been performed on the other carbon atoms of graphene with MM2 force fields, $E_{ONIOM} = E_{High} + E_{Medium} + E_{Low}$, (Scheme 2) [31].

On the other hand, the three-layered method of ONIOM lets us to discover a larger system more exactly than the one-layered model which could behave a medium-size system precisely like a ground system with acceptable accuracy [32, 33]. In this article, the structures have been calculated using the density-functional theory (DFT) on the mechanisms of adsorption of H_2S and SO_2 by TM (Fe, Ni, Zn) doping of Gr@NS through bonding between transition metals (Fe, Ni, Zn) and gas molecules of $H-\ddot{S}:-H$ and $:\ddot{O}=\ddot{S}=\ddot{O}:$. It has been found that the surface binding site preference of S-atom of H_2S and SO_2 in adsorption site is largely affected by the presence of neighboring atoms in the graphene sheet. The calculated $H_2S/SO_2 \rightarrow$ Fe-doped/Gr, $H_2S/ SO_2 \rightarrow$ Ni-doped/Gr, and $H_2S/SO_2 \rightarrow$ Zn-doped/Gr pair distribution functions have indicated that the formation of clusters directs to shorter $S \rightarrow$ Fe, $S \rightarrow$ Ni, and
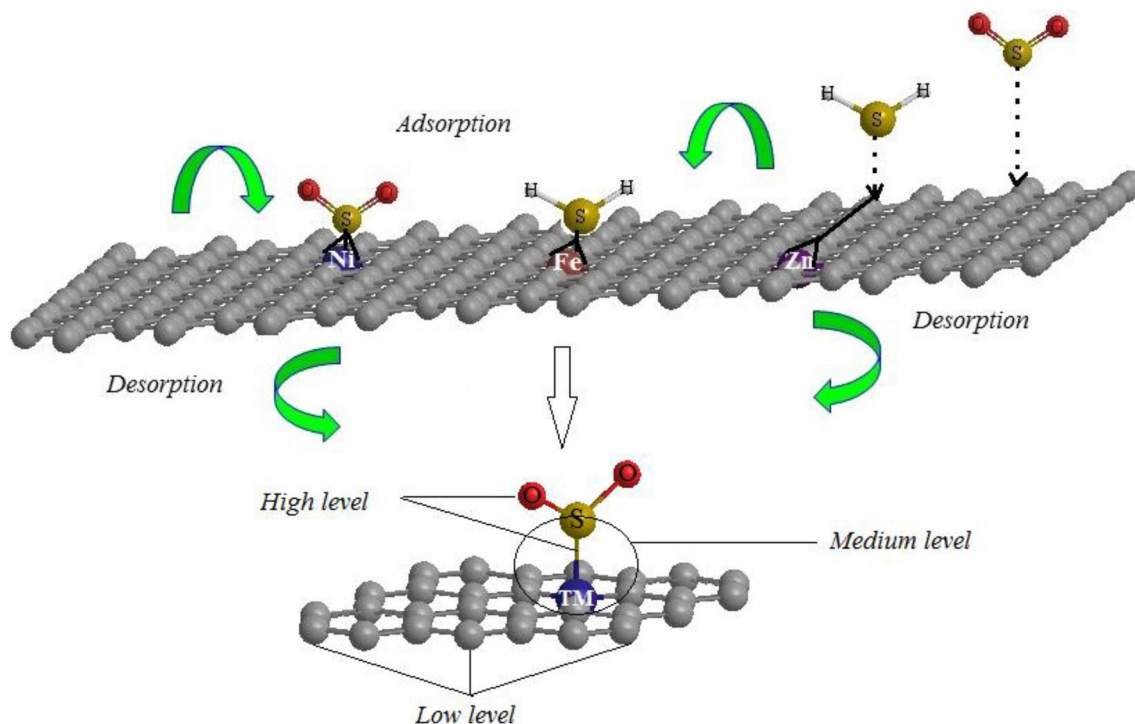
Scheme 2 The mechanism of the Langmuir adsorption of H_2S and SO_2 as the toxic gas pollutant onto TM (Fe, Ni, Zn) doping of Gr@NS based on optimized coordination due to three layers of high, medium, and low levels of ONIOM method

$S \rightarrow Zn$ bond lengths when compared to the homogeneous growth (Scheme 2).

Hybrid functional is a group of approximations for the exchange–correlation energy functional in DFT (Density-Functional Theory) which combines a part of exact exchange from HF (Hartree–Fock theory) method with the rest of the exchange–correlation energy from other information such as empirical or ab initio methodologies. Therefore, the exact exchange energy functional is illustrated by the Kohn–Sham orbitals instead of the density, so is placed as the indirect density functional. This study has applied the influence of the hybrid functional of three-parameter basis set of B3LYP (Becke, Lee, Yang, Parr) within the framework of DFT upon theoretical calculations [34, 35]. Transition metal doping of Gr@NS has been built by rigid system and Z-Matrix format of which a blank line has been placed and after that the following information has been illustrated. The rigid PES has been performed at CAM-B3LYP functional [36] and employing LANL2DZ /6–31 + G (d,p) basis sets to assign HOMO, LUMO, Mulliken charges, nuclear magnetic resonance properties, dipole moment, thermodynamic characteristics, and other quantum properties for this study [37] for H_2S and SO_2 adsorbed onto TM doping of Gr@NS, including $H_2S/SO_2 \rightarrow$ Fe-doped/Gr, $NO \rightarrow$ Ni-doped/Gr, and $H_2S/ SO_2 \rightarrow$ Zn-doped/Gr using Gaussian 16 program package [38].

2.4 PDOS Graphs and Electronic Properties Analysis

To further study the influence of the adsorbed transition metal atoms on the electronic properties of the TM (Fe, Ni, Zn)-doped graphene nanosheet, the projected density of states (PDOS) have been calculated and plotted in Scheme 3a–f. A distinct metallic feature can be observed in the TM (Fe, Ni, Zn)-doped graphene nanosheet because of the strong interaction between the p states of C in graphene sheet and the d state of Fe, Ni, and Zn near the Fermi energy. Moreover, the existence of covalent features for these alloys has exhibited the identical energy amount and figure of the PDOS for the p orbitals of C and d orbitals of Fe, Ni, and Zn (Scheme 3a–f).

Scheme 3a–c shows that the Fe, Ni, and Zn states doping of the graphene nanosheet through H_2S adsorption have more contributions at the middle of the conduction band between -5 eV and -15 eV, while contributions of Fe states are expanded (Scheme 3a), but Ni states (Scheme 3b) and Zn states (Scheme 3c) have minor contributions.

Besides, Fig. 3d–f indicates that the Fe, Ni, and Zn states doping of the graphene nanosheet through SO_2 adsorption have more contributions at the middle of the conduction band between -5 eV and -15 eV, while contribution of Fe states (Scheme 3d), but Ni states (Scheme 3e) and Zn states (Scheme 3f) have major contributions.
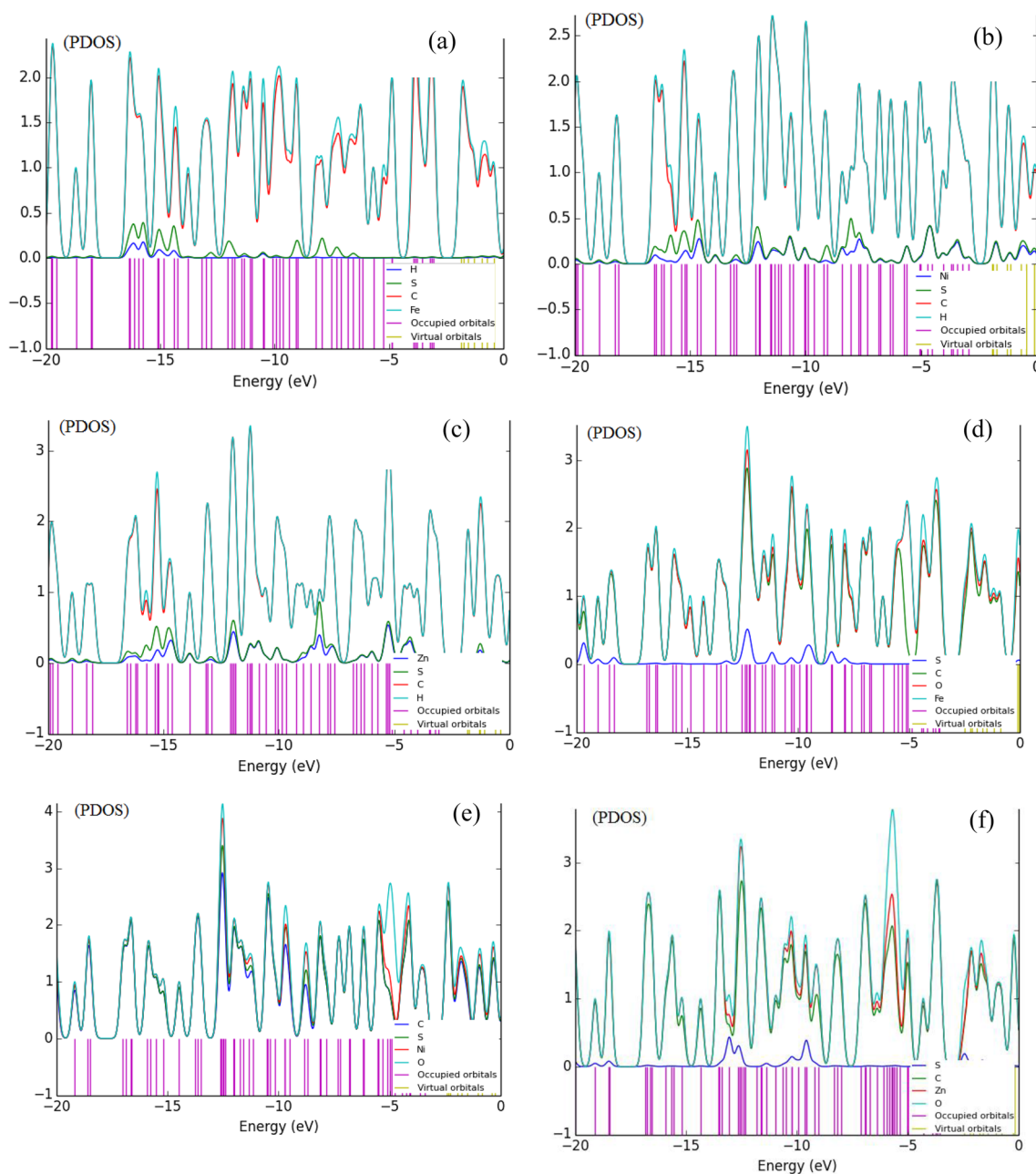
Scheme 3 The projected density of states of **a** Fe-doped, **b** Ni-doped, and **c** Zn-doped graphene nanosheet through H_2S adsorption and **d** Fe-doped, **e** Ni-doped, and **f** Zn-doped graphene nanosheet through SO_2 adsorption

Moreover, the results of the projected density of states (PDOS) have showed a certain charge association between the graphene nanosheet and doped elements of Fe, Ni, and Zn. In other words, the Fe states have large contributions in the valence band, while Ni and Zn states have fewer contributions. Thus, the cluster dominant of non-metallic and metallic features and a certain degree of covalent features can illustrate the increasing of the semiconducting direct band gap of (Fe, Ni, Zn)-doped graphene nanosheet.

3 Results and Discussion

In this investigation, transition metals such as iron, nickel, and zinc doped on the graphene nanosheet have been investigated as the efficient surface for adsorption of toxic gases H_2S and SO_2 causing air pollution. These experiments have been conducted by spectroscopy analysis through some physical and chemical properties.

3.1 NMR Spectroscopy and NBO Analysis

Isotropic (σ_{iso}) and anisotropy (σ_{aniso}) shielding tensors of NMR spectroscopy for certain atoms in the active site of H_2S and SO_2 adsorbed by the Fe, Ni, and Zn doping of Gr@NS through the formation of the binding between gas molecule and solid surface have been calculated using Gaussian 16 program software and reported in Tables 1 and 2 [38, 39].

In Fig. 1, it has been indicated the chemical shielding (ppm) of NMR graphs versus atom type through adsorption of H_2S and SO_2 onto the Fe-doped/Gr, Ni-doped/Gr, and Zn-doped/Gr nanosheet.

The graphs of NMR spectroscopy in Fig. 1a–c and a'–c' have shown approximately the identical chemical shielding behavior of isotropic and anisotropy parameters for H_2S/$SO_2 \rightarrow$ Fe-doped/Gr@NS (Fig. 1a, a') and H_2S/$SO_2 \rightarrow$ Ni-doped/Gr@NS (Fig. 1b, b'), with a sharp peak close to linkage of Fe-doped and Ni-doped on the surface of graphene with sulfur atom of H_2S and SO_2, respectively. Although, in the NMR spectroscopy, it has been observed the sharp peak around Zn-doped on the H_2S/$SO_2 \rightarrow$ Zn-doped/Gr@NS, there

Table 1 Calculated NMR chemical shielding tensors for some atoms in the active site of H_2S gas adsorption on the TM (Fe, Ni, Zn) doping of Gr@NS

H – S̈ : −H→ Fe–C				H – S̈ : −H→ Ni–C				H – S̈ : −H→ Zn–C			
Atom	Q	σ_{iso}	σ_{aniso}	Atom	Q	σ_{iso}	σ_{aniso}	Atom	Q	σ_{iso}	σ_{aniso}
S1	0.086	1357.60	1669.10	S1	0.1389	1460.88	304.55	S1	0.1980	1219.99	1427.20
C2	− 0.072	922.98	2519.02	C2	0.0911	911.05	1713.03	C2	0.0887	452.78	2527.32
C3	− 0.1038	1006.58	5038.25	C3	− 0.0598	141.01	1715.83	C3	− 0.0689	935.13	2307.05
C4	0.0009	730.93	4018.72	C4	− 0.0348	1628.87	7917.32	C4	− 0.0375	1954.01	8118.54
C5	0.0135	47.97	298.99	C5	− 0.0373	38.99	337.74	C5	− 0.0436	189.51	762.66
C6	− 0.084	1108.77	3771.01	C6	− 0.0691	664.22	1677.11	C6	− 0.0538	1171.96	3159.05
C7	− 0.4958	386.62	641.54	C7	− 0.4734	3.33	858.47	C7	− 0.3035	537.08	561.22
C8	− 0.1313	73.40	798.34	C8	− 0.0731	418.46	685.87	C8	− 0.0736	67.43	880.75
C9	− 0.1274	84.75	847.55	C9	− 0.0748	15.35	375.39	C9	− 0.0694	68.78	936.87
C10	− 0.0709	1301.33	2541.68	C10	0.0919	758.10	2470.30	C10	0.0882	525.47	2948.73
C11	− 0.0442	398.94	428.76	C11	− 0.0336	40.08	201.76	C11	− 0.0383	251.60	677.60
C12	0.0039	1613.65	3114.52	C12	− 0.0538	970.38	7626.75	C12	− 0.0514	1881.83	8159.34
C13	0.0026	439.23	677.69	C13	0.0138	11.98	469.69	C13	0.0129	194.59	719.04
C14	− 0.5473	710.11	1293.81	C14	− 0.4920	39.11	722.24	C14	− 0.3300	191.40	1403.72
C15	− 0.5586	714.16	1292.89	C15	− 0.4810	6.14	915.36	C15	− 0.3475	136.60	864.70
Fe16	1.9106	37,028.84	63,893.30	Ni16	1.4824	3654.86	18,290.63	Zn16	1.0288	689.66	6082.44
C17	0.0168	65.19	269.10	C17	− 0.0225	30.71	282.68	C17	− 0.0389	141.13	593.43
C18	− 0.0824	1144.40	3733.05	C18	− 0.0971	468.77	3494.69	C18	− 0.0515	1284.41	3351.30
C19	− 0.0507	109.39	175.84	C19	− 0.0556	68.37	210.69	C19	− 0.0581	16.96	1159.31
C20	− 0.0319	2427.00	5879.40	C20	− 0.0382	789.29	3294.29	C20	− 0.0404	1747.24	5216.77
C21	0.0653	307.27	674.99	C21	0.0501	40.84	168.63	C21	0.0480	174.67	454.76
C22	− 0.0824	5.96	329.86	C22	− 0.0673	196.51	46.15	C22	− 0.0665	0.5622	312.02
C23	− 0.0466	402.85	436.87	C23	− 0.0352	11.65	259.49	C23	− 0.0398	247.07	620.98
C24	− 0.0004	326.81	764.71	C24	0.0323	163.16	543.22	C24	0.0108	164.27	537.33
C25	0.0038	1433.10	2959.34	C25	− 0.0440	906.61	5544.93	C25	− 0.0475	1613.21	6064.71
C26	− 0.0003	637.07	3685.42	C26	− 0.0309	845.45	5344.31	C26	− 0.0369	1334.42	6433.95
C27	− 0.0159	2149.02	3098.26	C27	− 0.0312	75.33	1138.23	C27	− 0.0365	1031.24	2717.39
C28	0.1550	1099.63	5221.32	C28	0.1369	26.69	555.78	C28	0.1328	562.52	4517.43
C29	0.1548	930.34	5022.46	C29	0.1356	44.31	653.74	C29	0.1323	791.12	5000.39
C30	− 0.0510	120.46	340.95	C30	− 0.0558	104.43	237.41	C30	− 0.0579	12.71	1048.38
C31	− 0.0330	2347.04	6376.77	C31	− 0.0400	796.46	2973.31	C31	− 0.0434	1671.42	4543.91
H32	0.1166	64.43	95.12	H32	0.1190	37.32	28.74	H32	0.0979	36.02	31.11
H33	0.1004	81.71	95.74	H33	0.1087	38.99	27.42	H33	0.0969	37.43	26.47

Chemical shielding (CS) tensors in principal axes system evaluate the isotropic chemical shielding (σ_{iso}) and anisotropic chemical shielding (σ_{aniso}) [40]: $\sigma_{iso} = \frac{\sigma33 + \sigma22 + \sigma11}{3}$; $\sigma_{aniso} = \sigma33 - \frac{\sigma22 + \sigma11}{2}$

Table 2 Calculated NMR chemical shielding tensors for some atoms in the active site of SO_2 gas adsorption on the TM (Fe, Ni, Zn) doping of Gr@NS

$: \ddot{O} = \ddot{S} = \ddot{O} :\rightarrow$ Fe–C				$: \ddot{O} = \ddot{S} = \ddot{O} :\rightarrow$ Ni–C				$: \ddot{O} = \ddot{S} = \ddot{O} :\rightarrow$ Zn–C			
Atom	Q	σ_{iso}	σ_{aniso}	Atom	Q	σ_{iso}	σ_{aniso}	Atom	Q	σ_{iso}	σ_{aniso}
S1	0.2183	6842.87	14,501.72	S1	0.3176	6872.46	9461.32	S1	0.4539	9099.97	26,843.78
O2	− 0.2528	7622.27	17,547.49	O2	− 0.2638	6604.59	10,434.69	O2	− 0.2404	3421.95	30,612.79
O3	− 0.3061	6273.17	9827.58	O3	− 0.2836	6520.34	12,777.95	O3	− 0.2466	9945.21	17,272.88
C4	0.0964	9827.57	9827.57	C4	0.1495	1038.95	4066.74	C4	0.1435	493.48	6741.62
C5	− 0.0569	3208.04	10,380.43	C5	− 0.0197	2219.87	4221.71	C5	− 0.0383	6741.62	6523.36
C6	0.0047	884.67	3006.66	C6	− 0.0178	198.38	3249.34	C6	− 0.0235	535.20	5504.00
C7	0.0046	172.11	524.05	C7	− 0.0138	84.96	342.70	C7	− 0.0219	4.74	1020.67
C8	− 0.0512	1333.72	3989.11	C8	− 0.0652	707.13	1984.76	C8	− 0.0482	6618.09	24,895.19
C9	− 0.4104	2.99	3641.24	C9	− 0.4627	1168.16	1796.86	C9	− 0.3041	421.78	1893.52
C10	− 0.1027	489.70	949.02	C10	− 0.0410	182.19	1416.55	C10	− 0.0425	208.40	2958.02
C11	− 0.1063	229.92	1219.09	C11	− 0.0452	348.66	1180.622	C11	− 0.0473	369.93	2834.03
C12	0.0943	3118.30	4660.09	C12	0.1470	514.85	3858.48	C12	0.1420	1718.78	5325.34
C13	− 0.0301	464.76	828.07	C13	− 0.0207	183.64	489.80	C13	− 0.0345	116.67	632.68
C14	0.0076	720.51	2072.28	C14	− 0.0265	907.21	2418.86	C14	− 0.0180	1451.34	5479.92
C15	0.0193	391.60	1006.48	C15	0.0446	12.04	237.27	C15	0.03621	247.44	723.60
C16	− 0.4938	447.70	1267.72	C16	− 0.4637	373.21	786.04	C16	− 0.3599	430.56	1063.43
C17	− 0.5104	651.31	1387.21	C17	− 0.4781	221.72	221.72	C17	− 0.3532	474.95	2127.96
Fe18	1.6806	22,673.89	90,625.53	Ni18	1.4692	24,551.86	25,710.21	Zn18	1.04039	1403.82	10,646.56
C19	0.0223	67.70	343.29	C19	− 0.0092	305.77	811.18	C19	− 0.0299	15.47	1861.02
C20	− 0.0451	622.55	3843.05	C20	− 0.0603	559.20	1792.03	C20	− 0.0508	9121.24	36,956.95
C21	− 0.0472	234.80	565.89	C21	− 0.0479	127.04	958.14	C21	− 0.0514	149.67	1028.17
C22	− 0.0248	3472.00	9946.48	C22	− 0.0333	789.75	3063.75	C22	− 0.0409	52.02	8909.97
C23	0.0734	302.03	667.93	C23	0.0574	120.93	404.66	C23	0.0551	100.15	694.65
C24	− 0.0620	16.60	325.29	C24	− 0.0458	74.50	416.38	C24	− 0.0531	1.19	565.11
C25	− 0.0330	382.26	1006.68	C25	− 0.0178	248.51	816.57	C25	− 0.03	40.20	828.71
C26	0.0365	400.05	1301.46	C26	0.0472	192.08	492.75	C26	0.0422	6.07	1017.77
C27	0.0219	662.32	1536.38	C27	− 0.0178	731.93	11,396.09	C27	− 0.0285	1918.88	9669.13
C28	0.0086	941.78	2703.11	C28	− 0.0113	3763.64	9104.71	C28	− 0.0266	1448.02	9230.94
C29	− 0.0118	2134.49	3109.21	C29	− 0.0176	737.74	2377.10	C29	− 0.0269	689.14	2828.80
C30	0.1634	1984.09	6570.17	C30	0.1543	810.69	3850.66	C30	0.1447	421.60	5007.96
C31	0.1633	2.51	3822.05	C31	0.1533	80.97	442.79	C31	0.1453	868.94	4125.14
C32	− 0.0463	566.73	1234.85	C32	− 0.0462	79.65	1002.59	C32	− 0.0517	238.92	1342.82
C33	− 0.0242	5055.42	8544.17	C33	− 0.0309	1766.33	7340.41	C33	− 0.0346	2028.22	6488.28

Chemical shielding (CS) tensors in principal axes system evaluate the isotropic chemical shielding (σ_{iso}) and anisotropic chemical shielding (σ_{aniso}) [40]: $\sigma_{iso} = \frac{\sigma 33 + \sigma 22 + \sigma 11}{3}$; $\sigma_{aniso} = \sigma 33 - \frac{\sigma 22 + \sigma 11}{2}$

are some fluctuations in the chemical shielding behaviors of isotropic and anisotropy parameters (Fig. 1c, c′).

Furthermore, the Natural Bond Orbital (NBO) analysis of H_2S and SO_2 adsorbed on the TM (Fe, Ni, Zn) doping of Gr@NS has illustrated the character of electronic conjugation between bonds in the gas molecules and TM doping of Gr@NS (Table 3; Fig. 2).

In Fig. 2, it has been observed the fluctuation of occupancy of natural bond orbitals for $H_2S/SO_2 \rightarrow$ Fe-doped, $H_2S/SO_2 \rightarrow$ Ni-doped, and $H_2S/SO_2 \rightarrow$ Zn-doped graphene nanosheet through the Langmuir adsorption process by

indicating the active sulfur atom in hydrogen sulfide (H_2S) and sulfur dioxide (SO_2) becoming close to the nanosheet. Bond orbitals of C14—Ni 16 and C9—Ni in the adsorption of H_2S and SO_2, respectively, in the Ni doping of Gr@NS have shown the maximum occupancy.

3.2 Thermodynamic Properties and IR Spectroscopy Analysis

Thermodynamic parameters have been estimated for adsorption of Sulfur Dioxide ($: \ddot{O} = \ddot{S} = \ddot{O} :$) and Hydrogen

Fig. 1 NMR spectroscopy for adsorption of H_2S and SO_2 on the TM-doped graphene sheet, including **a** $H_2S \rightarrow Fe-C$, **a′** $SO_2 \rightarrow Fe-C$, **b** $H_2S \rightarrow Ni-C$, **b′** $SO_2 \rightarrow Ni-C$, **c** $H_2S \rightarrow Zn-C$, and **c′** $SO_2 \rightarrow Zn-C$
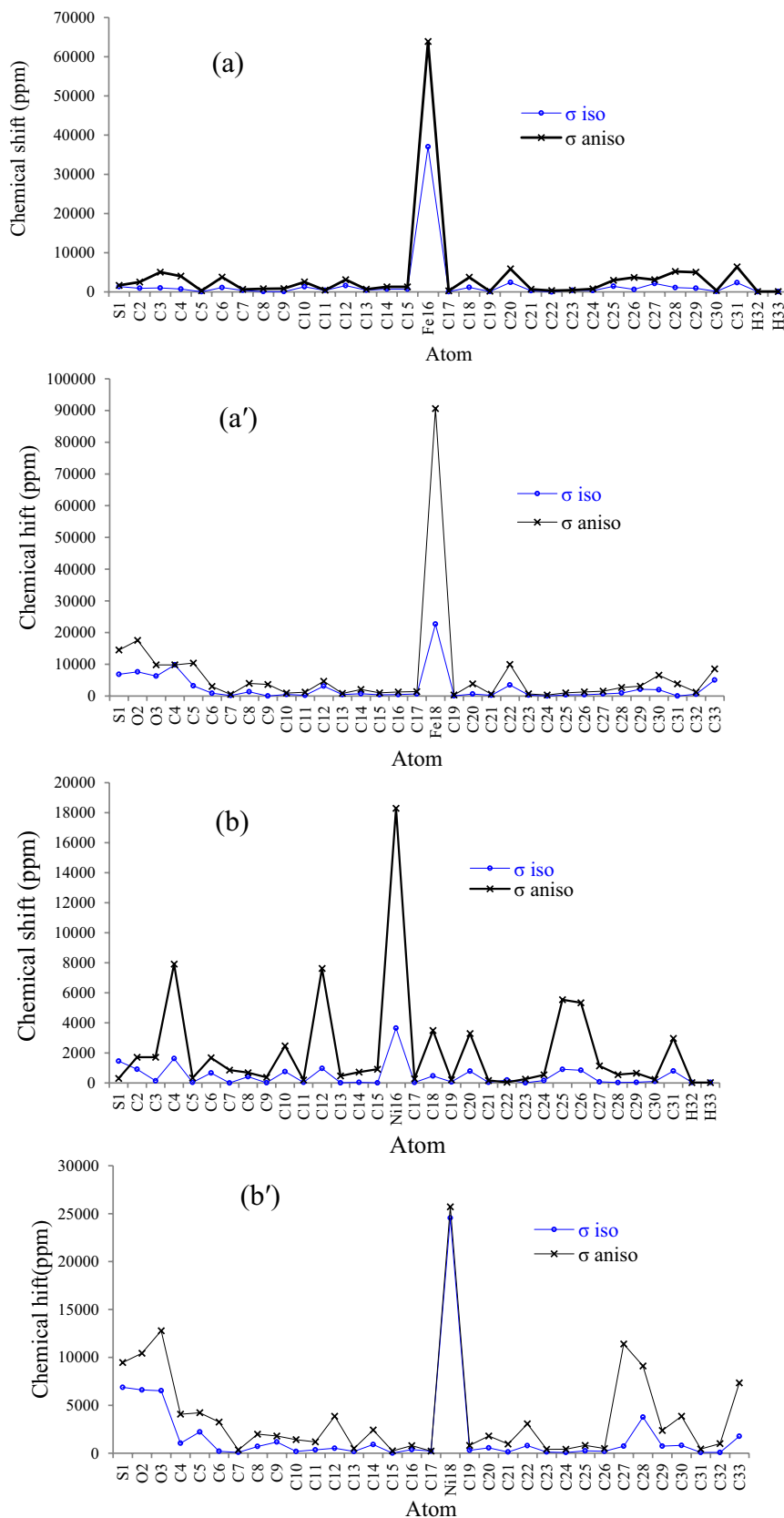
Fig. 1 (continued)
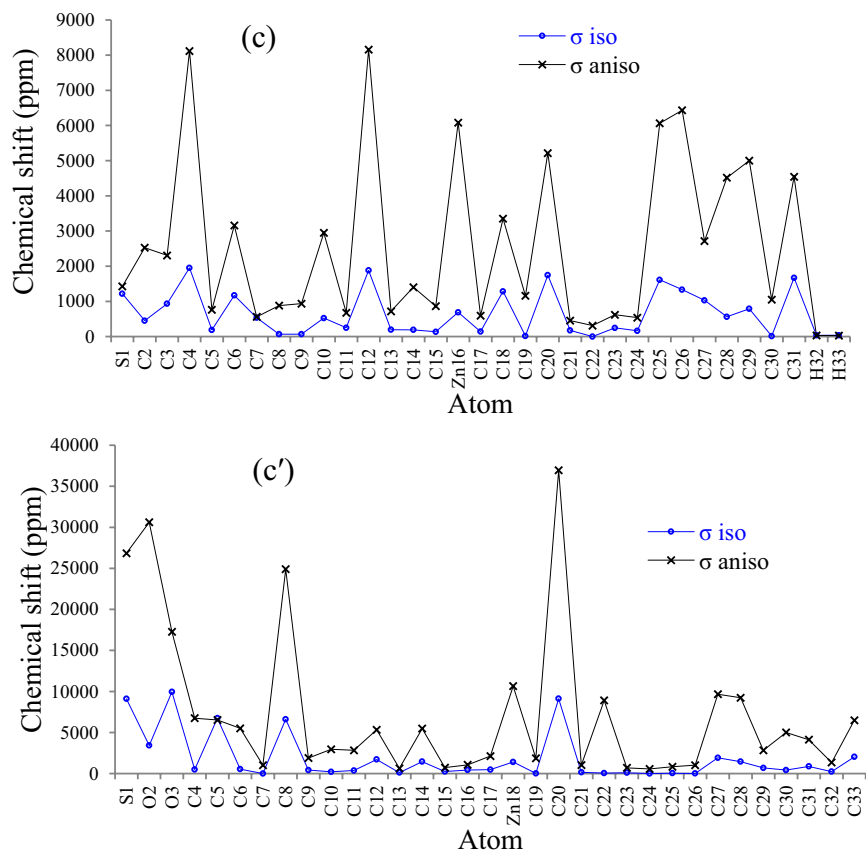
Table 3 NBO analysis for H_2S and SO_2 on the TM (Fe, Ni, Zn) doping of Gr@NS

NO → TM-doped/Gr nanosheet	Bond orbital	Occupancy	Hybrids
$H-S:-H \to$ Fe–C	BD (1) C7—Fe16	1.96225	0.8099 (sp$^{1.64}$) C + 0.5866 (sp$^{0.43}$ d$^{4.40}$) Fe
	BD (1) C14—Fe16	1.96398	0.8201 (sp$^{1.37}$) C + 0.5722 (sp$^{0.47}$ d$^{4.30}$) Fe
	BD (1) C15—Fe16	1.96295	0.8211 (sp$^{1.35}$) C + 0.5708 (sp$^{0.5\,0}$d$^{4.36}$) Fe
$H-\ddot{S}:-H \to$ Ni–C	BD (1) C7—Ni16	1.93134	0.8263 (sp$^{1.20}$) C + 0.5633 (sp$^{2.07}$ d$^{3.58}$) Ni
	BD (1) C14—Ni16	1.96992	0.8142 (sp$^{1.33}$) C + 0.5805 (sp$^{1.34}$ d$^{4.68}$)Ni
	BD (1) C15—Ni16	1.91797	0.8325 (sp$^{0.99}$) C + 0.5540 (sp$^{3.28}$ d$^{2.29}$) Ni
$H-\ddot{S}:-H \to$ Zn–C	BD (1) C7—Zn16	1.94341	0.8147 (sp$^{1.03}$) C + 0.5798 (sp$^{2.22}$ d$^{0.62}$) Zn
	BD (1) C14—Zn16	1.94172	0.8098 (sp$^{1.12}$) C + 0.5867 (sp$^{2.03}$ d$^{0.71}$)Zn
	BD (1) C15—Zn16	1.93933	0.8082 (sp$^{1.14}$) C + 0.5889 (sp$^{2.02}$ d$^{0.78}$) Zn
	BD (1) C9—Fe18	1.95918	0.8206 (sp$^{1.42}$) C + 0.5715 (sp$^{0.56}$ d$^{3.46}$) Fe
$:\ddot{O}=\ddot{S}=\ddot{O}: \to$ Fe–C	BD (1) C16—Fe18	1.95380	0.8118 (sp$^{1.40}$) C + 0.5840 (sp$^{0.73}$ d$^{3.97}$) Fe
	BD (1) C17—Fe18	1.95431	0.8101 (sp$^{1.40}$) C + 0.5863 (sp$^{0.63}$ d$^{4.03}$) Fe
	BD (1) C9—Ni18	1.97205	0.8057 (sp$^{1.41}$) C + 0.5923 (sp$^{0.75}$ d$^{4.17}$) Ni
$:\ddot{O}=\ddot{S}=\ddot{O}: \to$ Ni–C	BD (1) C16—Ni18	1.93258	0.7842 (sp$^{1.51}$) C + 0.6205 (sp$^{0.98}$ d$^{3.43}$) Ni
	BD (1) C17—Ni18	1.94565	0.7871 (sp$^{1.52}$) C + 0.6168 (sp$^{0.92}$ d$^{3.92}$) Ni
	BD (1) C9—Zn18	1.94453	0.8135 (sp$^{1.05}$) C + 0.5815 (sp$^{2.37}$ d$^{0.68}$) Zn
$:\ddot{O}=\ddot{S}=\ddot{O}: \to$ Zn–C	BD (1) C16 -Zn18	1.93721	0.7783 (sp$^{1.42}$) C + 0.6279 (sp$^{1.20}$ d$^{1.74}$) Zn
	BD (1) C17—Zn18	1.95268	0.7894 (sp$^{1.30}$) C + 0.6138 (sp$^{1.64}$ d$^{1.41}$) Zn

Sulfide ($H-\ddot{S}:-H$) on the surfaces of (Fe, Ni, Zn) doping of Gr@NS as the gas sensors which can be used as the selective detectors for toxic gases (Table 4).

Moreover, the infrared spectra for adsorption of H_2S and SO_2 by (Fe, Ni, Zn) doping of Gr@NS have been reported in Fig. 3a–c and a′–c′. Each of these graphs has been seen in the

Fig. 2 Occupancy fluctuation extracted of NBO method for bond orbitals of C–Fe, C–Ni, and C–Zn in Table 3 through adsorption of H_2S and SO_2 on the TM (Fe, Ni, Zn) doping of Gr@NS
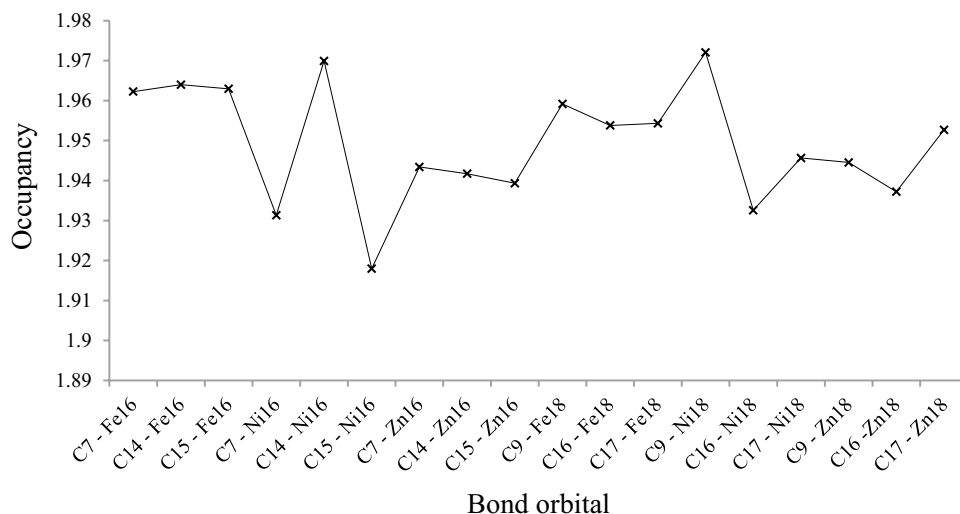
frequency range around 500–2000 cm^{-1} for the complexes of $H-\ddot{S}:-H\to$ Fe–C, $H-\ddot{S}:-H\to$ Ni–C, $H-\ddot{S}:-H\to$ Zn–C and $:\ddot{O}=\ddot{S}=\ddot{O}:\to$ Fe–C, $:\ddot{O}=\ddot{S}=\ddot{O}:\to$ Ni–C, and $:\ddot{O}=\ddot{S}=\ddot{O}:\to$ Zn–C.

Figure 3a and a′ shows the strongest IR peaks for $H-\ddot{S}:-H\to$ Fe–C and $:\ddot{O}=\ddot{S}=\ddot{O}:\to$ Fe–C approximately between 800 and 1000 cm^{-1}. Besides, it has seen the frequencies of 1600 cm^{-1} and 700 cm^{-1} for strongest peaks of $H-\ddot{S}:-H\to$ Ni–C and $:\ddot{O}=\ddot{S}=\ddot{O}:\to$ Ni–C, respectively (Fig. 3b, b′). Furthermore, the most frequencies of sharp peak for $H-\ddot{S}:-H\to$ Zn–C (two peaks) and $:\ddot{O}=\ddot{S}=\ddot{O}:\to$ Zn–C have been represented around 750 cm^{-1}, 1600 cm^{-1}, and 750 cm^{-1}, respectively (Fig. 3c, c′).

From Fig. 4, it could be found that the maximum of the Langmuir adsorption isotherm plots based on ΔG^o_{ads} versus dipole moment may depend on the interactions between the H_2S and SO_2 and the TM doping of Gr@NS. The order of Gibbs free energy changes of SO_2 adsorption on TM-doped Gr@NS is $\Delta G^0_{SO2\to Zn-C} > \Delta G^0_{SO2\to Ni-C} > \Delta G^0_{SO2\to Fe-C}$ and

also the order of Gibbs free energy changes of the clusters of $H_2S\to$ TM doping of Gr@NS is $\Delta G^0_{H2S\to Zn-C} > \Delta G^0_{H2S\to Ni-C} > \Delta G^0_{H2S\to Fe-C}$ (Fig. 4).

The adsorptive capacity of H_2S and SO_2 on the TM doping of Gr@NS is approved by the ΔG^o_{ads} amounts. $\Delta G^o_{ads} = \Delta G^o_{NO\to TM-C} - (\Delta G^o_{NO} + \Delta G^o_{TM-C})$; TM = Fe, Ni, Zn.

On the basis of data in Table 4, it is predicted that the adsorption of H_2S and SO_2 on the TM doping of Gr@NS must be physical and chemical nature. As shown in Fig. 4, all the computed ΔG^o_{ads} amounts are very close, which exhibits the agreement of the evaluated data by all methods and the validity of the computations.

Fig. 4 indicates that $\Delta G^o_{ads,H2S\to Fe-C}$ and $\Delta G^o_{ads,SO2\to Fe-C}$ have the largest gap of Gibbs free energy adsorption with dipole moment which defines the changes between Gibbs free energy of initial compounds ($\Delta G^o_{H2S}/\Delta G^o_{Fe-C}$) and ($\Delta G^o_{SO2}/\Delta G^o_{Fe-C}$) and product compounds ($\Delta G^o_{H2S\to Fe-C}$) and ($\Delta G^o_{SO2\to Fe-C}$) through polarizability. In fact, TM-doped/Gr

Table 4 The physico-chemical properties of H_2S and SO_2 adsorbed by the Fe, Ni, and Zn doping of Gr@NS as the selective gas sensor

Compound	$\Delta E^o \times 10^{-4}$ (kcal/mol)	$\Delta H^o \times 10^{-4}$ (kcal/mol)	$\Delta G^o \times 10^{-4}$ (kcal/mol)	S^o (Cal/K.mol)	Dipole moment (Debye)
Fe–C	− 146.2783	− 146.2782	− 146.2816	111.175	2.3199
Ni–C	− 162.4794	− 162.4793	− 162.4828	116.150	13.6226
Zn–C	− 178.2031	− 178.2030	− 178.2066	120.533	1.7301
$H-\ddot{S}:-H$	− 24.7417	− 24.7417	− 24.7432	50.421	1.0267
$H-\ddot{S}:-H\to$ Fe–C	− 171.0112	− 171.0111	− 171.0149	125.858	14.8980
$H-\ddot{S}:-H\to$ Ni–C	− 186.1527	− 186.1526	− 186.1561	118.420	7.2222
$H-\ddot{S}:-H\to$ Zn–C	− 202.9333	− 202.9332	− 202.9368	121.125	5.7742
$:\ddot{O}=\ddot{S}=\ddot{O}:$	− 33.9252	− 33.9251	− 33.9269	60.100	2.1632
$:\ddot{O}=\ddot{S}=\ddot{O}:\to$ Fe–C	− 180.1926	− 180.1925	− 180.1965	134.972	8.6680
$:\ddot{O}=\ddot{S}=\ddot{O}:\to$ Ni–C	− 195.3362	− 195.3361	− 195.3401	133.549	3.8136
$:\ddot{O}=\ddot{S}=\ddot{O}:\to$ Zn–C	− 212.1156	− 212.1156	− 212.1194	128.542	2.2208
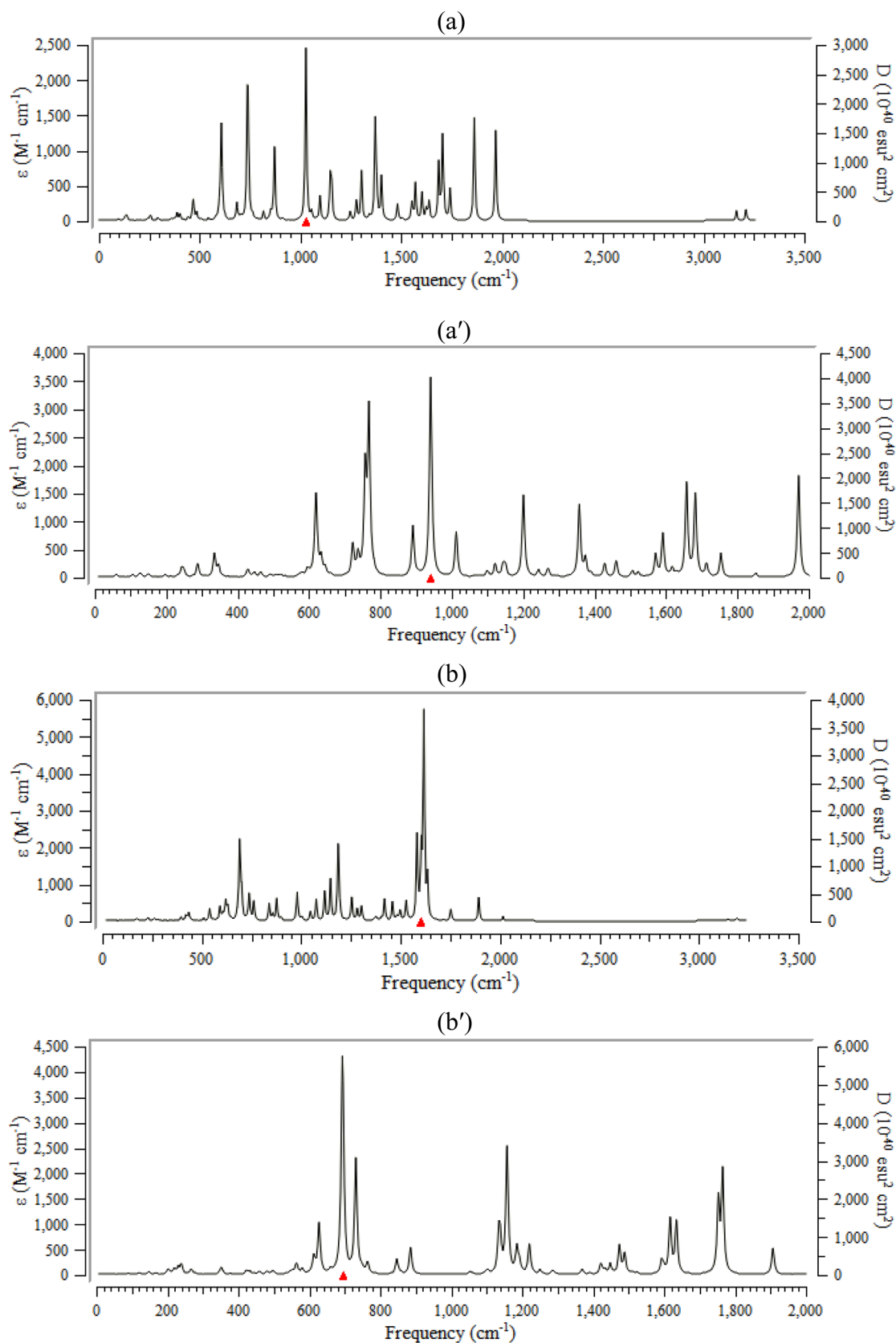
Fig. 3 Changes of Frequency (cm^{-1}) through the IR spectra for **a** H$_2$S→Fe-, **a′** SO$_2$→Fe-, **b** H$_2$S→Ni-, **b′** SO$_2$→Ni-, **c** H$_2$S→Zn-, and **c′** SO$_2$→Zn-doped graphene nanosheet as the selective gas detector
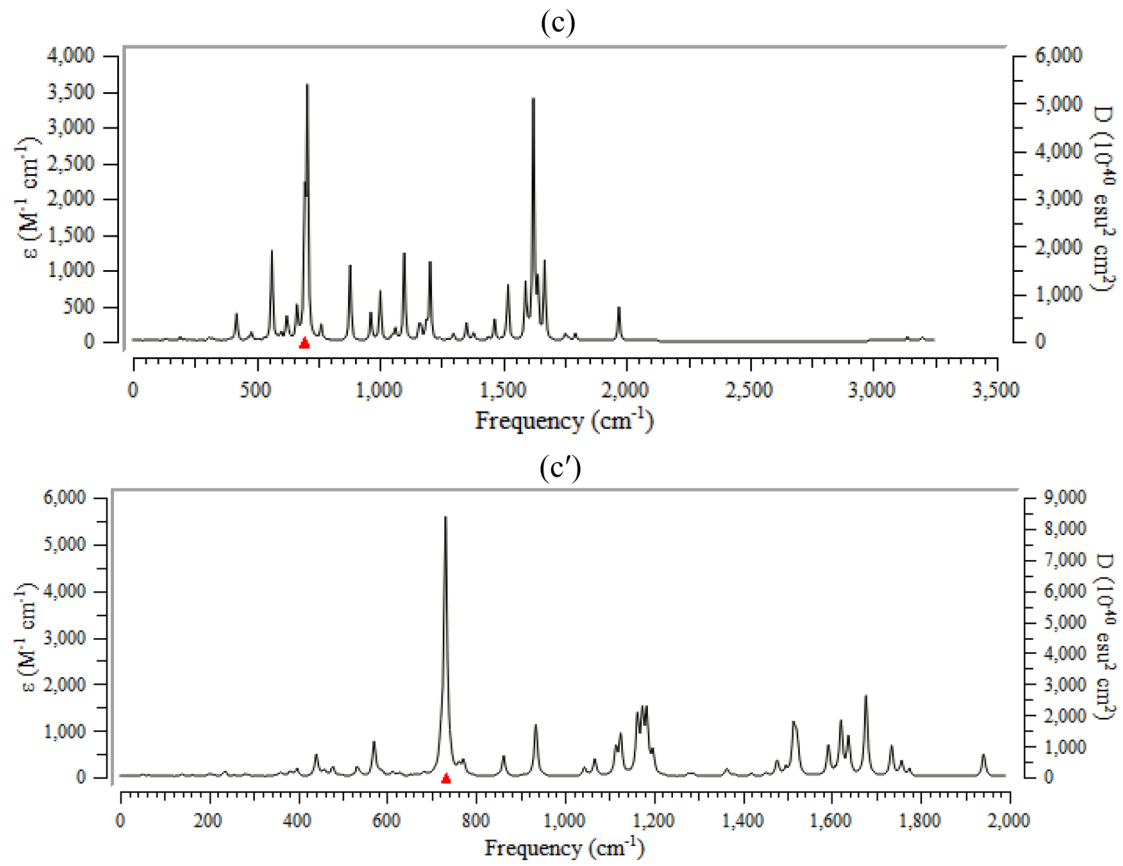
(c)

(c′)

Fig. 3 (continued)

Fig. 4 The changes of Gibbs free energy for adsorption of H$_2$S and SO$_2$ as the toxic gases on the TM (Fe, Ni, Zn) doping of Gr@NS
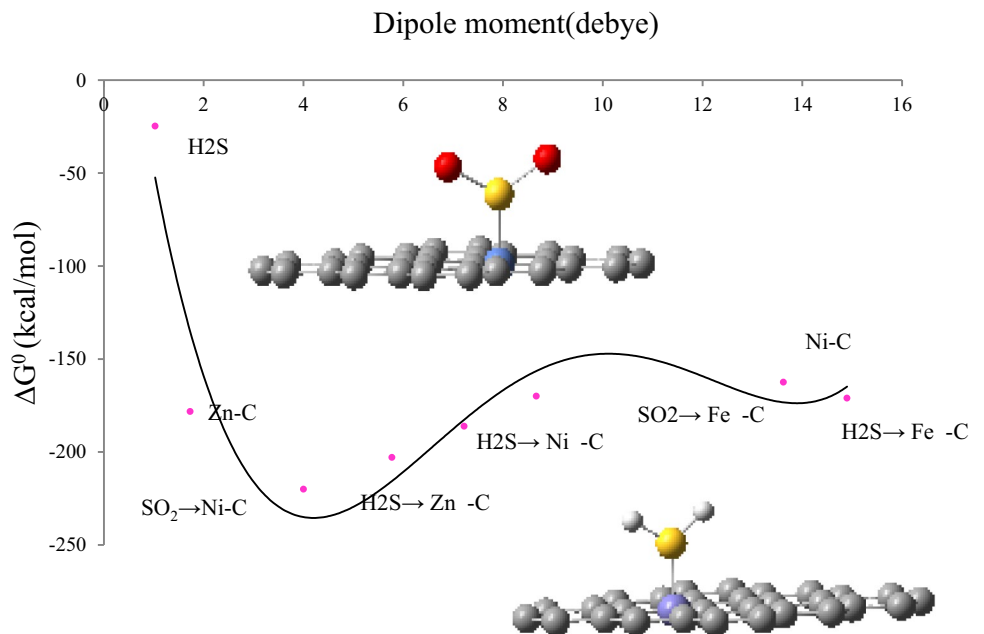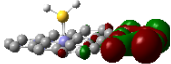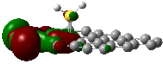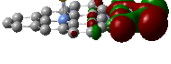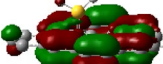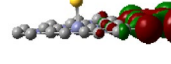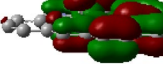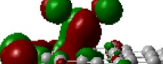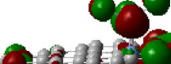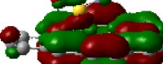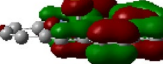
Table 5 The HOMO (a.u.), LUMO (a.u.), band energy gap (ΔE /ev), and other quantities (ev) for adsorption of H_2S and SO_2 as the toxic gases on the TM (Fe, Ni, Zn) doping of Gr@NS using CAM-B3LYP/ LANL2DZ, 6–31+G (2d,p)

Gas→TM-doped Gr@NS	LUMO	HOMO	ΔE	μ	χ	η	ζ	ψ
H – S̈ : –H→ Fe–C	-0.00735	-0.11658	2.9723	− 1.6861	1.6861	1.4861	0.3364	0.9565
H – S̈ : –H→ Ni–C	0.01708	-0.13609	4.1679	− 1.6192	1.6192	2.0839	0.2399	0.6290
H – S̈ : –H→ Zn–C	0.02368	-0.15810	4.9464	− 1.8288	1.8288	2.4732	0.2021	0.6761
: Ö = S̈ = Ö :→ Fe–C	-0.00805	-0.15567	4.0169	− 2.2275	2.2275	2.0084	0.2489	1.2352
: Ö = S̈ = Ö :→ Ni–C	-0.00141	-0.16035	4.3249	− 2.2008	2.2008	2.1624	0.2312	1.1199
: Ö = S̈ = Ö :→ Zn–C	0.00058	-0.16909	4.6169	− 2.2927	2.2927	2.3084	0.2166	1.1385

$\Delta E = E_{LUMO} - E_{HOMO}$; $\mu = (E_{HOMO} + E_{LUMO})/2$; $\chi = - (E_{HOMO} + E_{LUMO})/2$; $\eta = (E_{LUMO} - E_{HOMO})/2$; $\zeta = 1/(2\eta)$; and $\psi = \mu^2/(2\eta)$

can possess enough efficiency for adsorption toxic gases of hydrogen sulfide and sulfur dioxide through charge transfer from sulfur to the transition metal.

3.3 Frontier Molecular Orbitals of HOMO, LUMO, and UV–VIS Analysis

The highest occupied molecular orbital (HOMO) energy is generated by ionization and the lowest unoccupied molecular orbital (LUMO) energy is observed by the electron affinity. These parameters have been evaluated for adsorption of hydrogen sulfide and sulfur dioxide on the TM (Fe, Ni, Zn) doping of Gr@NS as the gas detector in Table 5. The HOMO (au), LUMO (au), and band energy gap ($\Delta E = E_{LUMO} - E_{HOMO}$) (ev) have exhibited the pictorial explanation of the frontier molecular orbitals and their respective positive and negative areas which are a significant parameter for discovering the molecular properties of

Fig. 5 UV–VIS spectra for **a**
$H_2S \rightarrow$Fe-doped, **a′** $SO_2 \rightarrow$Fe-doped, **b** $H_2S \rightarrow$Ni-doped, **b′**
$SO_2 \rightarrow$Ni-doped, **c** $H_2S \rightarrow$Zn-doped, and **c′** $SO_2 \rightarrow$Zn-doped
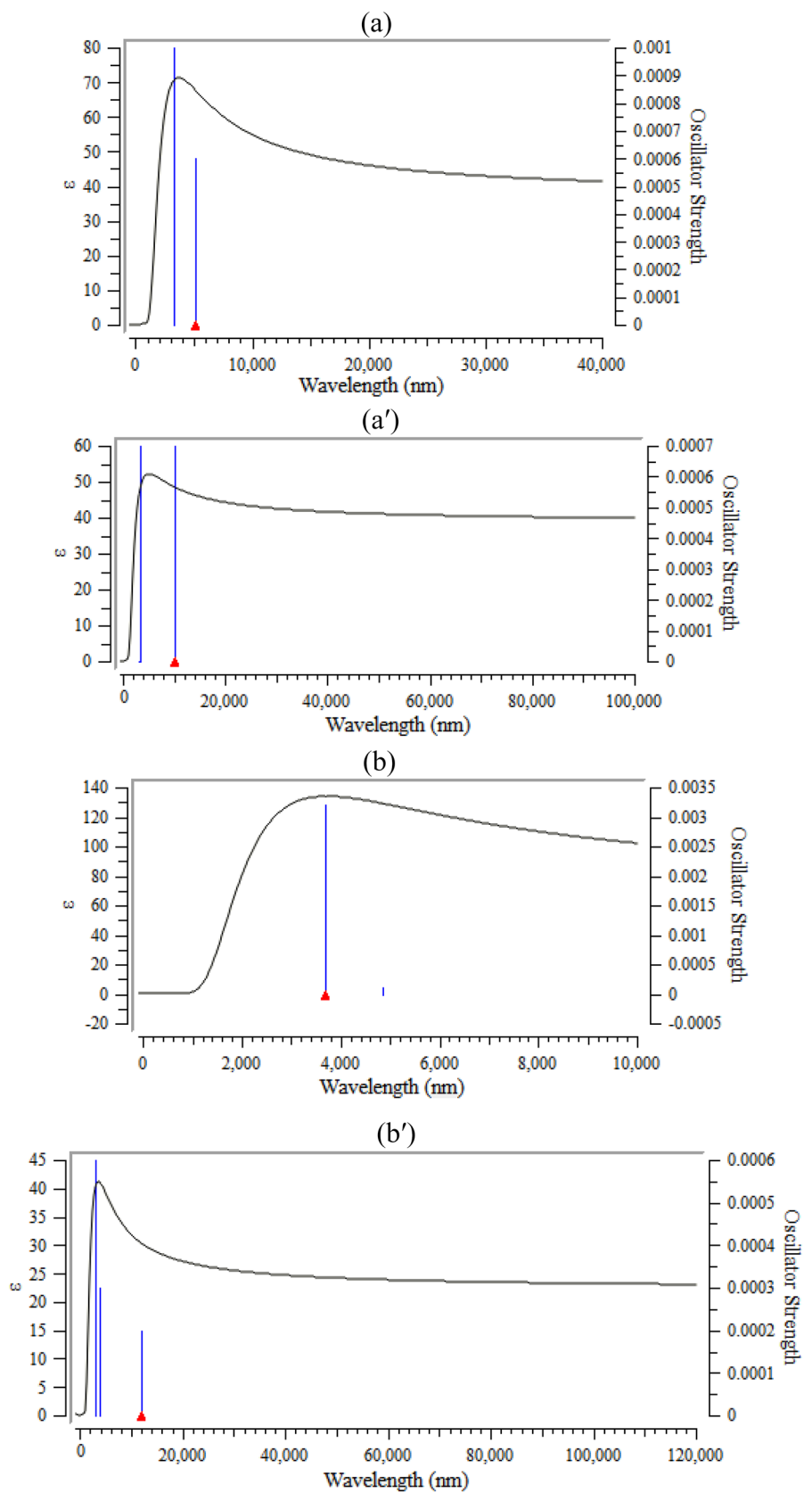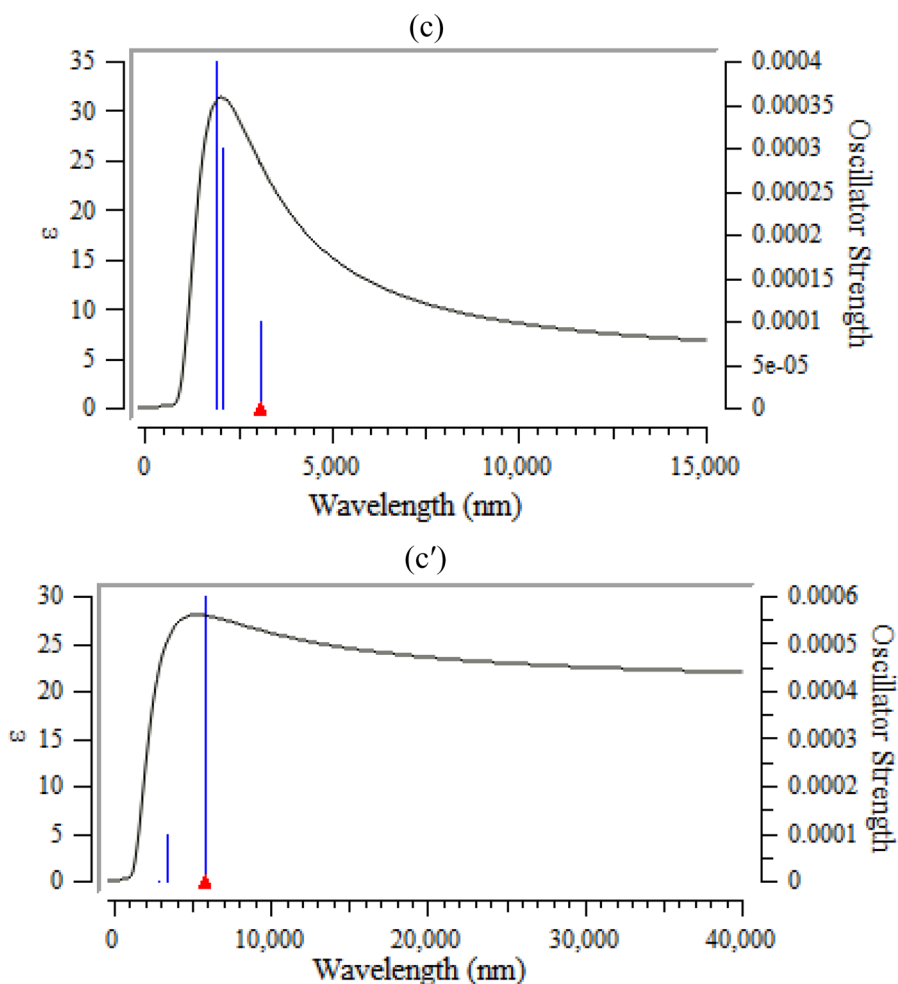on the graphene nanosheet

Fig. 5 (continued)

(c)

(c′)

efficient compounds in the adsorption of H_2S and SO_2 on the TM doping of Gr@NS (Table 5).

Moreover, for getting more conclusive approval in identifying the compound characteristics of adsorption complexes of $H_2S/$ $SO_2 \rightarrow$ TM (Fe, Ni, Zn) doping of Gr@NS, a series of chemical reactivity parameters such as chemical potential (μ), electronegativity (χ), hardness (η), softness (ζ), and electrophilicity index (ψ) have been carried out (Table 5) [41–43].

On the other hand, the HOMO shows the capability for giving an electron, while the LUMO as an electron acceptor exhibits the capability for achieving an electron. Therefore, the energy gap ($\Delta E = E_{LUMO} - E_{HOMO}$) indicates the energy difference between frontier HOMO and LUMO orbital introducing the stability for the structure and unravels the chemical activity of the molecule. In this work, energy gap establishes how toxic gas of H_2S and SO_2 can be adsorbed on the TM (Fe, Ni, Zn) doping of Gr@NS as the gas sensor at B3LYP/LANL2DZ, 6–311 + G (2d, p) quantum method. Besides, frontier molecular orbitals play an important function in the optical and electrical properties, like in UV–VIS spectra [44].

The energy gap between HOMO and LUMO has distinguished the attributes of molecular electrical transport [45]. Through Frank–Condon principle, the maximum absorption peak (max) depends on an UV–visible spectrum to vertical excitation.

The negative values of the chemical potential (μ) versus the positive values of other amounts have displayed an appropriate efficiency of scavenging H_2S and SO_2 by TM (Fe, Ni, Zn) doping of Gr@NS.

In addition, TD-DFT/ LANL2DZ, 6–31 + G (2d, p) computations have been done to identify the low-lying excited states of H_2S and SO_2 adsorbed on the TM (Fe, Ni, Zn) doping of Gr@NS. The results consist of the vertical excitation energies, oscillator strength, and wavelength which have been introduced in Fig. 5a–c and a′–c′.

Figure 5a–c and a′–c′ have shown UV–VIS spectra for $H_2S \rightarrow$ Fe-doped, $H_2S \rightarrow$ Ni-doped, and $H_2S \rightarrow$ Zn-doped graphene sheet with maximum adsorption bands between 2000 and 5000 nm. Moreover, it has observed the maximum adsorption around 2000 and 10000 nm for $SO_2 \rightarrow$ Fe-doped, $SO_2 \rightarrow$ Ni-doped, and $SO_2 \rightarrow$ Zn-doped graphene sheet (Fig. 5a–c, a′–c′).

4 Conclusion

This research aimed to remark the study of polluting gases such as hydrogen sulfide and sulfur dioxide adsorption employing graphene nanosheet. The graphene sheet reviewed in general physically adsorb many of the pollutant gas molecules considered and the interaction can usually enhance by transition metal doping which ameliorates their detecting properties through chemisorption study. This article has reported the trends for H_2S and SO_2 chemisorption on transition metal (iron, nickel, and zinc) doping of Gr@NS. In particular, the energetic, structural, and infrared adsorption characteristics of linearly (atop) H_2S and SO_2 adsorbed on (Fe, Ni, Zn)-doped graphene nanosheet have been discovered. Spin-unrestricted density-functional theory (DFT) calculations were applied to verdict the tendency of H_2S and SO_2 adsorption energy ($H_2S/SO_2 \rightarrow$ Fe-doped, $H_2S/SO_2 \rightarrow$ Ni-doped, and $H_2S/SO_2 \rightarrow$ Zn-doped on the Gr nanosheet) and N–O vibrational frequency (ν_{NO}) for clusters composed of Fe, Ni, and Zn. The effects of the transition metal electronic structure on the adsorption energy of H_2S and SO_2, and how these chemical factors might be related to the catalytic activity of transition-supported metal catalysts that deal with the adsorption, and surface diffusion, have been investigated. Therefore, the cluster dominant of non-metallic and metallic features and a certain degree of covalent features can indicate the enhancement of the semiconducting direct band gap of transition metal doping of graphene nanosheet which can conduct us toward the electronic structure, relative stability, and surface bonding of various metal-doped graphene nanosheet, metal alloy surfaces, and other related mechanisms of friction lubrication and biological systems.

Declarations

Conflict of interest The authors declare no conflict of interest.

Ethical Approval The authors consent to participate and publish the data.

References

1. Kroto HW, Heath JR, O'Brien SC, Curl RF, Smalley RE (1985) C60: Buckminsterfullerene. Nature 318:162–163
2. Nasibulin AG, Pikhitsa PV, Jiang H, Brown DP, Krasheninnikov AV, Anisimov AS, Queipo P, Moisala A, Gonzalez D, Lientschnig G et al (2007) A novel hybrid carbon material. Nat Nanotechnol 2:156–161
3. Mollaamin F, Shahriari S, Monajjemi M et al (2023) Nanocluster of aluminum lattice via organic inhibitors coating: a study of Freundlich adsorption. J Clust Sci 34(3):1547–1562. https://doi.org/10.1007/s10876-022-02335-1
4. Moisala A, Nasibulin AG, Shandakov SD, Jiang H, Kauppinen EI (2005) On-line detection of single-walled carbon nanotube formation during aerosol synthesis methods. Carbon 43:2066–2074
5. Mollaamin F, Monajjemi M (2023) Transition metal (X = Mn, Fe Co, Ni, Cu, Zn)-doped graphene as gas sensor for CO_2 and NO_2 detection: a molecular modeling framework by DFT perspective. J Mol Model 29:119. https://doi.org/10.1007/s00894-023-05526-3
6. Delgado JL, Herranz M, Martín N (2008) The nano-forms of carbon. J Mater Chem 18:1417
7. Falcao EH, Wudl F (2007) Carbon allotropes: beyond graphite and diamond. J Chem Technol Biotechnol 82:524–531
8. Langenhorst F, Campione M (2019) Ideal and real structures of different forms of carbon, with some remarks on their geological significance. J Geol Soc 176:337–347
9. Mollaamin F, Monajjemi M (2023) Doping of graphene nanostructure with iron, nickel and zinc as selective detector for the toxic gas removal: a density functional theory study. C 9(1):20.https://doi.org/10.3390/c9010020.
10. Su Y, Wang J, Wang B, Yang T, Yang B, Xie G, Zhou Y, Zhang S, Tai H, Cai Z et al (2020) Alveolus-inspired active membrane sensors for self-powered wearable chemical sensing and breath analysis. ACS Nano 14:6067–6075. https://doi.org/10.1021/acsnano.0c01804
11. Ma D, Zhang J, Li X, He C, Lu Z, Lu Z, Lu Z, Yang Z, Wang Y (2018) C3N monolayers as promising candidates for NO_2 sensors. Sens Actuators B 266:664–673. https://doi.org/10.1016/j.snb.2018.03.159
12. Pacheco M, Pacheco J, Valdivia R, Santana A, Tu X, Mendoza D, Frias H, Medina L, Macias J (2017) Green applications of carbon nanostructures produced by plasma techniques. MRS Adv 2:2647–2659
13. Lee SW, Lee W, Hong Y, Lee G, Yoon DS (2018) Recent advances in carbon material-based NO_2 gas sensors. Sens Actuators B 255:1788–1804. https://doi.org/10.1016/j.snb.2017.08.203
14. Chatterjee SG, Chatterjee S, Ray AK, Chakraborty AK (2015) Graphene–metal oxide nanohybrids for toxic gas sensor: a review. Sens Actuators B 221:1170–1181. https://doi.org/10.1016/j.snb.2015.07.070
15. Xiao Z, Kong LB, Ruan S, Li X, Yu S, Li X, Jiang Y, Yao Z, Ye S, Wang C et al (2018) Recent development in nanocarbon materials for gas sensor applications. Sens Actuators B 274:235–267. https://doi.org/10.1016/j.snb.2018.07.040
16. Bakhshi K, Mollaamin F, Monajjemi M (2011) Exchange and correlation effect of hydrogen chemisorption on nano V(100) surface: a DFT study by generalized gradient approximation (GGA). J Comput Theor Nanosci 8:763–768. https://doi.org/10.1166/jctn.2011.1750
17. Mollaamin F, Monajjemi M (2023) Graphene embedded with transition metals for capturing carbon dioxide: gas detection study using QM methods. Clean Technol 5(1):403–417. https://doi.org/10.3390/cleantechnol5010020
18. Monajjemi M, Baie MT, Mollaamin F (2010) Interaction between threonine and cadmium cation in [Cd(Thr)] (n = 1–3)

complexes: density functional calculations. Russ Chem Bull 59:886–889. https://doi.org/10.1007/s11172-010-0181-5.

19. Khaleghian M, Zahmatkesh M, Mollaamin F, Monajjemi M (2011) Investigation of solvent effects on armchair single-walled carbon nanotubes: a QM/MD study. Fuller Nanotub Carbon Nanostruct 19:251–261. https://doi.org/10.1080/15363831003721757

20. Monajjemi M, Khaleghian M, Tadayonpour N, Mollaamin F (2010) The effect of different solvents and temperatures on stability of single-walled carbon nanotube: a QM/MD study. Int J Nanosci 09:517–529. https://doi.org/10.1142/S0219581X10007071

21. Shahriari S, Mollaamin F, Monajjemi M (2023) Increasing the performance of {[(1-x-y) LiCo0.3Cu0.7] (Al and Mg doped)] O2}, xLi2MnO3, yLiCoO2 composites as cathode material in lithium-ion battery: synthesis and characterization. Micromachines 14:241.https://doi.org/10.3390/mi14020241.

22. Mollaamin F, Monajjemi M (2015) Harmonic linear combination and normal mode analysis of semiconductor nanotubes vibrations. J Comput Theor Nanosci 12:1030–1039. https://doi.org/10.1166/jctn.2015.3846

23. Wen X, Bai P, Han Z, Zheng S, Luo B, Fang T, Song W (2019) Effect of vacancy on adsorption/dissociation and diffusion of H2S on Fe(1 0 0) surfaces: a density functional theory study. Appl Surf Sci 465:833–845. https://doi.org/10.1016/j.apsusc.2018.09.220

24. Mollaamin F, Monajjemi M (2023) In silico-DFT investigation of nanocluster alloys of Al-(Mg, Ge, Sn) coated by nitrogen heterocyclic carbenes as corrosion inhibitors. J Clust Sci. https://doi.org/10.1007/s10876-023-02436-5

25. Mollaamin F, Monajjemi M (2023) Molecular modelling framework of metal-organic clusters for conserving surfaces: Langmuir sorption through the TD-DFT/ONIOM approach. Mol Simul 49(4):365–376. https://doi.org/10.1080/08927022.2022.2159996

26. Wen X, Bai P, Shuqi Zheng Yu, Tian, (2021) Adsorption and dissociation mechanism of hydrogen sulfide on layered FeS surfaces: a dispersion-corrected DFT study. Appl Surf Sci 537:147905. https://doi.org/10.1016/j.apsusc.2020.147905

27. Wen X, Bai P, Liang J, Zheng S, Tian Y (2022) Slab model studies of H2S adsorption/dissociation and diffusion on pristine FeS(001) surfaces and FeS(001) surfaces with pre-adsorbed X atoms (X = H, O, and S). J Mater Res Technol. https://doi.org/10.1016/j.jmrt.2022.03.047

28. Hanaor DAH, Ghadiri M, Chrzanowski W, Gan Y (2014) Scalable surface area characterization by electrokinetic analysis of complex anion adsorption (PDF). Langmuir 30(50):15143–15152. https://doi.org/10.1021/la503581e

29. Boyd A, Dube I, Fedorov G, Paranjape M, Barbara P (2014) Gas sensing mechanism of carbon nanotubes: from single tubes to high-density networks. Carbon 69:417–423

30. Zhao J, Buldum A, Han J, Lu JP (2002) Gas molecule adsorption in carbon nanotubes and nanotube bundles. Nanotechnology 13:195–200

31. Svensson M, Humbel S, Froese RDJ, Matsubara T, Sieber S, Morokuma K (1996) ONIOM: a multilayered integrated MO + MM method for geometry optimizations and single point energy predictions. A test for diels−alder reactions and Pt(P(t-Bu)3)2 + H2 oxidative addition. J Phys Chem 100(50):19357–19363. https://doi.org/10.1021/jp962071j

32. Brandt F, Jacob CR (2022) Systematic QM region construction in QM/MM calculations based on uncertainty quantification. J Chem Theory Comput 18(4):2584–2596. https://doi.org/10.1021/acs.jctc.1c01093

33. Mollaamin F, Monajjemi M, Salemi S, Baei MT (2011) A dielectric effect on normal mode analysis and symmetry of BNNT nanotube. Fuller Nanotub Carbon Nanostruct 19:182–196. https://doi.org/10.1080/15363831003782932

34. Becke AD (1993) Density-functional thermochemistry. III. The role of exact exchange. J Chem Phys 98:5648–5652

35. Lee C, Yang W, Parr RG (1988) Development of the Colle-Salvetti correlation-energy formula into a functional of the electron density. Phys Rev B 37:785–789

36. Becke AD (1988) Density-functional exchange-energy approximation with correct asymptotic behavior. Phys Rev A 38:3098–3100

37. Ditchfield R, Hehre WJ, Pople JA (1971) Self-consistent molecular-orbital methods. IX. An extended Gaussian-type basis for molecular-orbital studies of organic molecules. J Chem Phys 54:724–728

38. Frisch MJ, Trucks GW, Schlegel HB, Scuseria GE, Robb MA, Cheeseman JR, Scalmani G, Barone V, Petersson GA, Nakatsuji H, Li X, Caricato M, Marenich AV, Bloino J, Janesko BG, Gomperts R, Mennucci B, Hratchian HP, Ortiz JV, Izmaylov AF, Sonnenberg JL, Williams-Young D, Ding F, Lipparini F, Egidi F, Goings J, Peng B, Petrone A, Henderson T, Ranasinghe D, Zakrzewski VG, Gao J, Rega N, Zheng G, Liang W, Hada M, Ehara M, Toyota K, Fukuda R, Hasegawa J, Ishida M, Nakajima T, Honda Y, Kitao O, Nakai H, Vreven T, Throssell K, Montgomery JAJr, Peralta JE, Ogliaro F, Bearpark MJ, Heyd JJ, Brothers EN, Kudin KN, Staroverov VN, Keith TA, Kobayashi R, Normand J, Raghavachari K, Rendell AP, Burant JC, Iyengar SS, Tomasi J, Cossi M, Millam JM, Klene M, Adamo C, Cammi R, Ochterski JW, Martin RL, Morokuma K, Farkas O, Foresman JB, Fox DJ (2016) Gaussian 16, Revision C.01, Gaussian, Inc., Wallingford CT

39. Tahan A, Mollaamin F, Monajjemi M (2009) Thermochemistry and NBO analysis of peptide bond: Investigation of basis sets and binding energy. Russ J Phys Chem A 83:587–597. https://doi.org/10.1134/S003602440904013X

40. Novotný J, Jan Vícha J, Bora PL, Repisky M, Straka M, Komorovsky S, Marek R (2017) Linking the character of the metal-ligand bond to the ligand NMR shielding in transition-metal complexes: NMR contributions from spin-orbit coupling. J Chem Theory Comput 13(8):3586–3601. https://doi.org/10.1021/acs.jctc.7b00444

41. Kohn W, Becke AD, Parr RG (1996) Density functional theory of electronic structure. J Phys Chem 100:12974–12980. https://doi.org/10.1021/jp960669l

42. Parr RG, Pearson RG (1983) Absolute hardness: companion parameter to absolute electronegativity. J Am Chem Soc 105:7512–7516. https://doi.org/10.1021/ja00364a005

43. Politzer P, Abu-Awwad F (1998) A comparative analysis of Hartree-Fock and Kohn-Sham orbital energies. Theor Chem Acc 99:83–87. https://doi.org/10.1007/s002140050307

44. Aihara J (1999) Reduced HOMO−LUMO gap as an index of kinetic stability for polycyclic aromatic hydrocarbons. J Phys Chem A 103(37):7487–7495. https://doi.org/10.1021/jp990092i

45. Silverstein RM, Bassler GC, Morrill TC (1981) Spectrometric identification of organic compounds, 5th edn. Wiley, New York

Authors and Affiliations

Fatemeh Mollaamin[1,2] · Majid Monajjemi[3]

✉ Fatemeh Mollaamin
smollaamin@gmail.com

[1] Department of Food Engineering, Faculty of Engineering and Architecture, Kastamonu University, Kastamonu, Turkey

[2] Department of Biology, Faculty of Science, Kastamonu University, Kastamonu, Turkey

[3] Department of Chemical Engineering, Central Tehran Branch, Islamic Azad University, Tehran, Iran